Korean J. Chem. Eng., 40(3), 657-666 (2023)
DOI: 10.1007/s11814-022-1241-x

pISSN: 0256-1115
eISSN: 1975-7220

Synthesis of ternary core-shell carbon sphere@α-Fe_2O_3@Ag composites and their application for simultaneous voltammetric detection of uric acid, xanthine, and hypoxanthine

Ho Van Minh Hai*, Dinh Quang Khieu, The Ky Vo*, Van Cuong Nguyen*,†, and Jinsoo Kim***,†**

*Faculty of Chemical Engineering, Industrial University of Ho Chi Minh City,
12 Nguyen Van Bao, Go Vap, Ho Chi Minh City, Vietnam
**Department of Chemistry, University of Sciences, Hue University, 530000, Vietnam
***Department of Chemical Engineering (Integrated Engineering), Kyung Hee University,
1732 Deogyeong-daero, Giheung-gu, Yongin-si, Gyeonggi-do 17104, Korea
(*Received 11 May 2022 • Revised 4 July 2022 • Accepted 26 July 2022*)

Abstract−Core-shell carbon sphere (CS)@α-Fe_2O_3@Ag was synthesized via a multistep hydrothermal method. First, the D-glucose hydrothermal process was employed to synthesize micron-size CSs on which α-Fe_2O_3 was grown to obtain the composite sphere of CS@α-Fe_2O_3. Thereafter, Ag^+ was reduced on the surface of the CS@α-Fe_2O_3 sphere using $NaBH_4$ agent to produce the core-shell CS@α-Fe_2O_3@Ag. Finally, microsphere composite CS@α-Fe_2O_3@Ag was coated on a glassy carbon electrode (GCE) to enhance its electrochemical performance in the simultaneous determination of uric acid (UA), xanthine (XN), and hypoxanthine (HP). Results indicated that the CS@α-Fe_2O_3@Ag-coated GCE exhibited improved voltammetric sensitivity toward UA, XN, and HP compared to bare GCE. The oxidation peak currents of the simultaneous detection of UA, XN, and HP increased linearly in the concentration range of 0.5-8.0 μmol L^{-1}. The detection limits of the fabricated electrodes for UA, XN, and HP were ~0.042, 0.089, and 0.048 μmol L^{-1}, respectively, being more sensitive than many other modified GCEs. Moreover, the CS@α-Fe_2O_3@Ag-coated GCE exhibited good stability and repeatability. This study opens a new perspective for developing highly efficient electrodes for electrochemical analysis.

Keywords: Carbon Sphere, Electrochemical Analysis, α-Fe_2O_3, UA, XN, HP, GCE, Voltammetry

INTRODUCTION

Uric acid (UA), xanthine (XN), and hypoxanthine (HP), which are the products of metabolism, are crucial in nerve functioning. These compounds also enormously impact animal metabolism and human circulating systems [1]. UA, also known as the major component in urine, is reportedly produced from the metabolism of endogenous (DNA and RNA) or exogenous purines. A high concentration of UA in the blood is so-called hyperuricemia or Lesh-Nyhan syndrome, which may result in gout and other pathological conditions, such as obesity, diabetes, high blood pressure, and kidney and heart diseases [2]. XN is known as an intermediate of purine nucleotide and deoxynucleotide metabolism. XN is usually used to treat obstructive sleep-disordered breathing in children [3]. Moreover, HP, which is a natural purine derivative, is usually used as the precursor of XN. It has been reported that HP plays a vital role in the adenosine exchange process, nucleic acid synthesis, and energy metabolism in human cells. Detecting UA, XN, and HP is reportedly essential for disease diagnosis and prevention. Therefore, many analytical methods have been applied for simultaneously detecting these components, such as ultraviolet-visible spectrophotometry, capillary electrophoresis, high-performance liquid chromatography, and electrochemical technique [4-8]. Among them, the electrochemical technique is considered promising as it is simple to operate and does not require complex sampling compared to other techniques. Nonetheless, the accuracy and efficiency of the electrochemical technique predominantly depend on the electrode's properties, such as electrical conductivity, sensitivity, or porosity. Therefore, developing efficient electrodes with high sensitivity and fast response toward UA, XN, and HP is necessary. Recently, the modification of the conventional glassy carbon electrode (GCE) to enhance its activity has received enormous attention. For instance, the GCE's surface modified with mesoporous graphitized carbon [9], sulfonic acid functionalized nitrogen-doped graphene [10], Co-doped CeO_2 nanoparticles (NPs) [11], or poly(pyrocatechol violet)/functionalized multi-walled carbon nanotubes composite film [12] have been applied for simultaneous detection of UA, XN, and HP. Studies have found that using these electrodes still has limitations due to interference from other redox-active species that have the same action potential, causing the overlap of voltammetric signals, lowered sensitivity, and reduced detection limit. To solve these problems, the modification of electrodes by coating with nanostructured materials with high electrical conductivity and abundant adsorptive sites is considered a promising solution. Among known coated materials, hierarchical core–shell nanostructured materials, such as metal oxide/metal oxide [13,14], metal oxide/metal hydroxide [15]

†To whom correspondence should be addressed.
E-mail: nvc@iuh.edu.vn, jkim21@khu.ac.kr

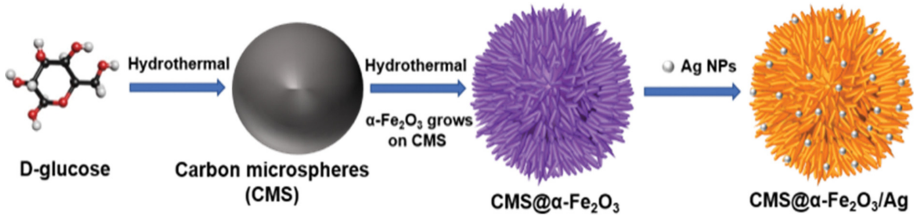

Scheme 1. A schematic of the formation of the core-shell CS@α-Fe_2O_3@Ag.

and carbon/metal oxide [16,17], have received considerable interest owing to their high conductivity, large specific surface area, and a highly ordered structure. Moreover, these hybrid core-shell nanostructures contain numerous adsorptive sites, which are favorable for capturing molecules on their surface. It has been reported that the electron transfer between an electrode and electrolyte is significantly enhanced when hybrid core-shell nanostructures are coated on the electrode's surface [18].

Recently, hematite (α-Fe_2O_3) has emerged as a promising material for developing electrochemical sensors due to its low cost, high specific surface area, and nontoxicity [19,20]. However, α-Fe_2O_3 exhibited poor electrical conductivity due to its low electrochemical performance [21]. It was found that the combination between α-Fe_2O_3 and carbon-based materials (e.g., graphene, carbon nanotubes, carbon fiber, or porous carbon) or metals (e.g., Au, Ag, or Pt) can improve its electrical conductivity [22-24]. In this study, a multistep hydrothermal process developed a ternary core-shell composite carbon sphere (CS)@α-Fe_2O_3@Ag with improved properties. First, micron-sized CSs were synthesized by D-glucose hydrothermal process. Then, α-Fe_2O_3 was self-assembled onto the surface of the CSs to form a binary core-shell CS@α-Fe_2O_3 structure via the seed-mediated growth method. Ag^+ was reduced on the surface of CS@α-Fe_2O_3 by $NaBH_4$ to fabricate a ternary core-shell CS@α-Fe_2O_3@Ag (Scheme 1). The fabricated CS@α-Fe_2O_3@Ag composite was coated onto the surface of GCE, which was then used as a working electrode for electrochemical performance of UA, XN, and HP. We realized that the CS@α-Fe_2O_3@Ag-coated GCE exhibited improved electrochemical performance in detecting UA, XN, and HP. The ternary core-shell CS@α-Fe_2O_3@Ag-modified electrode was developed and applied to detect UA, XN, and HP simultaneously.

EXPERIMENTAL

1. Materials

D-glucose ($C_6H_{12}O_6$, 99.5%), ferrous sulfate heptahydrate ($FeSO_4 \cdot 7H_2O$, 99%), silver nitrate ($AgNO_3$, 99%), sodium borohydride ($NaBH_4$, 99%), UA ($C_5H_4N_4O_3$, 99%), XN ($C_5H_4N_4O_2$, 99%), and HP ($C_5H_4N_4O$, 99%) were obtained from the Merck company, Germany. Potassium hydroxide (KOH), phosphoric acid (H_3PO_4, 85%), potassium dihydrogen phosphate (KH_2PO_4, 99%), and boric acid (H_3BO_3, 99%) were from Daejung, Korea. The Britton-Robinson buffer solutions were prepared by mixing 0.5-M H_3BO_3, 0.5-M H_3PO_4, and 0.5-M CH_3COOH. The desired pH value of the Britton-Robinson buffer was adjusted using KOH (1 M) or H_3PO_4 (1 M) solution.

2. Synthesis of Core-shell CS@α-Fe_2O_3

First, CS was prepared by dissolving 4.0-g glucose (0.022 mol) in 40-mL deionized (DI) water. Then, the resultant solution was transferred into a Teflon-lined autoclave and kept at 180 °C for 8 h. After the reaction, black products were collected and washed several times with DI water. The resulting product was dried at 60 °C for 24 h before use.

Binary core-shell CS@α-Fe_2O_3 nanocomposite was synthesized following a previous procedure with a slight modification [25]. Typically, 80-mg carbon microspheres were dispersed into 25-mL sodium acetate (0.05 M) with ultrasonication for 1 h. Then, 0.278-g $FeSO_4 \cdot 7H_2O$ (1 mmol) was added to the solution. Next, the mixture was transferred into a Teflon-lined autoclave and kept at 80 °C for 24 h. After the reaction, the mixture was naturally cooled to ambient temperature. The brown solid was collected and washed with DI water and ethanol several times. Then, the final product was dried at 60 °C overnight.

3. Synthesis of Ternary Core-shell CS@α-Fe_2O_3@Ag

The prepared CS@α-Fe_2O_3 (100 mg) was dispersed into 80-mL DI water under sonication for 10 min. Then, 5-mL $AgNO_3$ (1 mg mL^{-1}) was added dropwise to the solution and stirred for 30 minutes at ambient temperature. Next, 10-mL $NaBH_4$ (2 mg mL^{-1}) was added to the mixture. Afterward, the reaction mixture was aged for 24 h; the solid product was collected by centrifugation and washed several times with DI water and ethanol. The product was finally dried at 60 °C for 24 h. The prepared material was denoted as CS@α-Fe_2O_3@Ag.

4. Fabrication of CS@α-Fe_2O_3@Ag-coated GCE

First, the surface of the working GCE was initially polished with alumina slurry (0.05 μm), followed by careful washing with DI water and ethanol. The coating solution was prepared by dispersing 1-mg CS@α-Fe_2O_3@Ag nanocomposite into DI water with sonication to yield a stable suspension. Then, 5 μL of the resultant solution was coated onto the surface of the GCE, followed by drying naturally at ambient temperature for 2 h to obtain the CS@α-Fe_2O_3@Ag-coated GCE. For comparison, several electrodes, including CS-coated GCE and CS@α-Fe_2O_3-coated GCE, were also prepared following the same procedure.

5. Characterization

The crystallographic structure of the fabricated materials was analyzed using an X-ray diffraction (XRD) analyzer (MAC-18XHF, Rigaku, Japan) with Cu-Kα (λ=1.5406 Å) radiation. Morphological analyses of the samples were performed using a field emission scanning electron microscope (FE-SEM) (Leo-Supra 55, Carl Zeiss STM, Germany). Transmission electron microscopy (TEM) images were obtained using a JEOL JEM-2100 transmission electron micro-

scope at 200 kV. Fourier transformation infrared (FT-IR) analyses were recorded on a Shimadzu IRPrestige-21 (Japan). N_2 adsorption-desorption isotherms were measured at 77 K by a gas adsorption analyzer (Micromeritics 2020). Before being measured, the samples were degassed and vacuumed at 393 K for 8 h. The specific surface area of the samples was calculated via the multiple-point Brunauer-Emmett-Teller method.

6. Electrochemical Experiment

The fabricated CS-coated GCE, CS@α-Fe_2O_3-coated GCE, and CS@α-Fe_2O_3@Ag-coated GCE were used as working electrodes for simultaneous detection of UA, XN, and HP in their solution. Cyclic voltammetry (CV) and differential pulse voltammetry (DPV) were performed using a CPA-HH5 Computerized Polarography Analyzer (Vietnam). The auxiliary and reference electrodes were the platinum wire and Ag/AgCl (sat. KCl), respectively.

RESULTS AND DISCUSSION

1. Characterization

The formation mechanism of ternary core-shell carbon sphere@α-Fe_2O_3@Ag composites can be described as follows: First, α-Fe_2O_3 was self-assembled into the surface of carbon microspheres to form the binary core-shell CS@α-Fe_2O_3 composite through seed-mediated growth method. The reaction mechanism can be addressed as follows:

$$CH_3COO^- + H_2O \rightarrow CH_3COOH + OH^- \quad (1)$$

$$2Fe^{2+} + 6OH^- \rightarrow \alpha\text{-}Fe_2O_3 + 3H_2O \quad (2)$$

Eventually, Ag nanoparticles were incorporated into the surface shell layer of the binary CS@α-Fe_2O_3 composite owing to the reduction of $NaBH_4$ to produce hierarchically self-assembled CS@α-Fe_2O_3/Ag ternary core-shell composite. Morphological analyses of the fabricated CS, CS@α-Fe_2O_3 and CS@α-Fe_2O_3@Ag nanocomposite are shown in Fig. 1. The synthesized CS exhibited well-defined spheres with a smooth surface and particle size in the range of 0.2-0.5 μm [Fig. 1(a)]. Meanwhile, the obtained CS@α-Fe_2O_3 spheres exhibited a rough surface due to the growth of α-Fe_2O_3 on the CS's surface, resulting in the formation of core-shell structured CS@α-Fe_2O_3 [Fig. 1(b)]. Fig. 1(c) shows the SEM image of the ternary core-shell CS@α-Fe_2O_3@Ag sphere, revealing that the morphology changed slightly due to the deposition of Ag NPs on its surface. The resultant CS@α-Fe_2O_3@Ag remained spherical during the synthesis. The dot mapping analyses implied that C, O, Fe, and Ag were well-dispersed throughout the CS@α-Fe_2O_3@Ag sphere.

TEM analyses of the hierarchically self-assembled CS@α-Fe_2O_3@Ag are shown in Figs. 2(a)-(d). As shown, the prepared CS@α-Fe_2O_3@Ag comprised CS core and α-Fe_2O_3 shell with incorporated Ag NPs. The TEM images reveal that the lattice fingers of the shell layer have interplanar distances of 2.702, 2.519, and 1.703 nm, corresponding to the (104), (110), and (116) planes of hexagonal-structure α-Fe_2O_3 [Figs. 2(b)-(c)]. Notably, the α-Fe_2O_3 shell layer epitaxially grew on the CS's surface, producing a heterojunction within the CS@α-Fe_2O_3@Ag sphere. This structure is reportedly beneficial for the charge transfer process within the material, resulting in an enhancement of liquid electrolyte penetration and an efficient buffering for large volume changes during the charge/discharge process [26]. Fig. 2(d) shows the incorporation of Ag NPs onto α-Fe_2O_3 shell layer. As shown, the incorporated Ag NPs had lattice fingers with interplanar distances of ~2.358 and 2.024 nm,

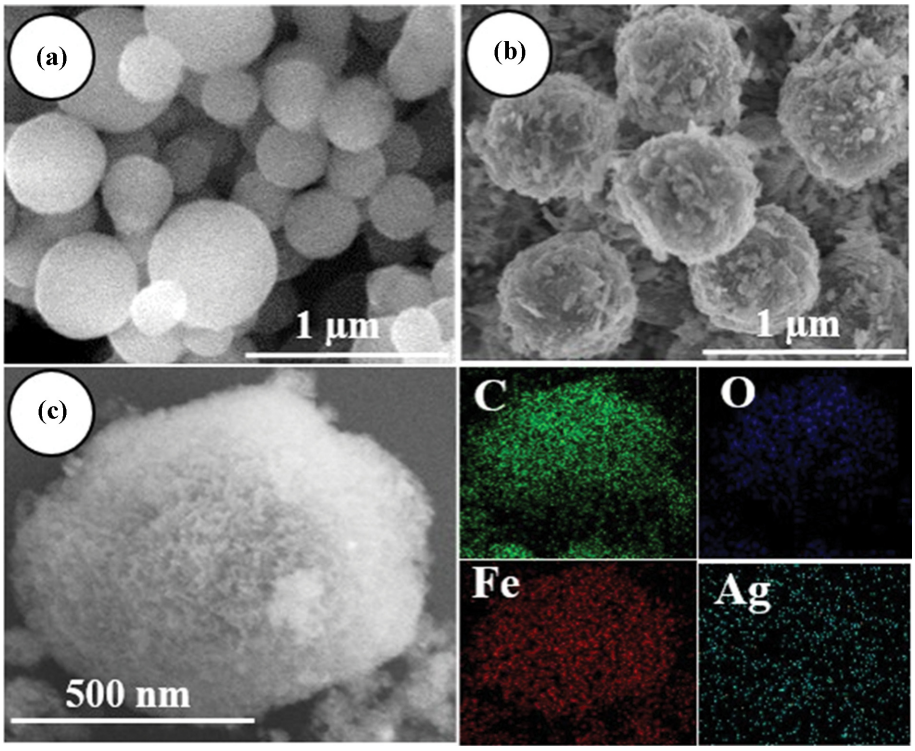

Fig. 1. SEM images of (a) CS, (b) CS@α-Fe_2O_3, and (c) CS@α-Fe_2O_3@Ag, with dot mappings of C, O, Fe, and Ag of CS@α-Fe_2O_3@Ag sample.

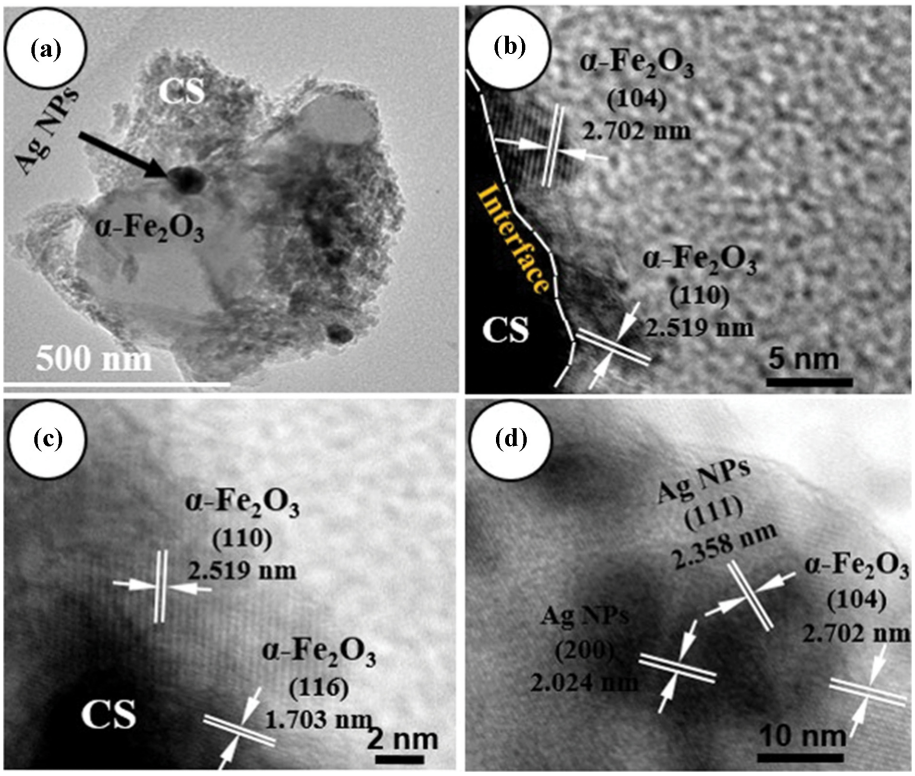

Fig. 2. (a) TEM image of CS@α-Fe_2O_3@Ag ternary core-shell composite, and (b)-(d) high-resolution TEM images.

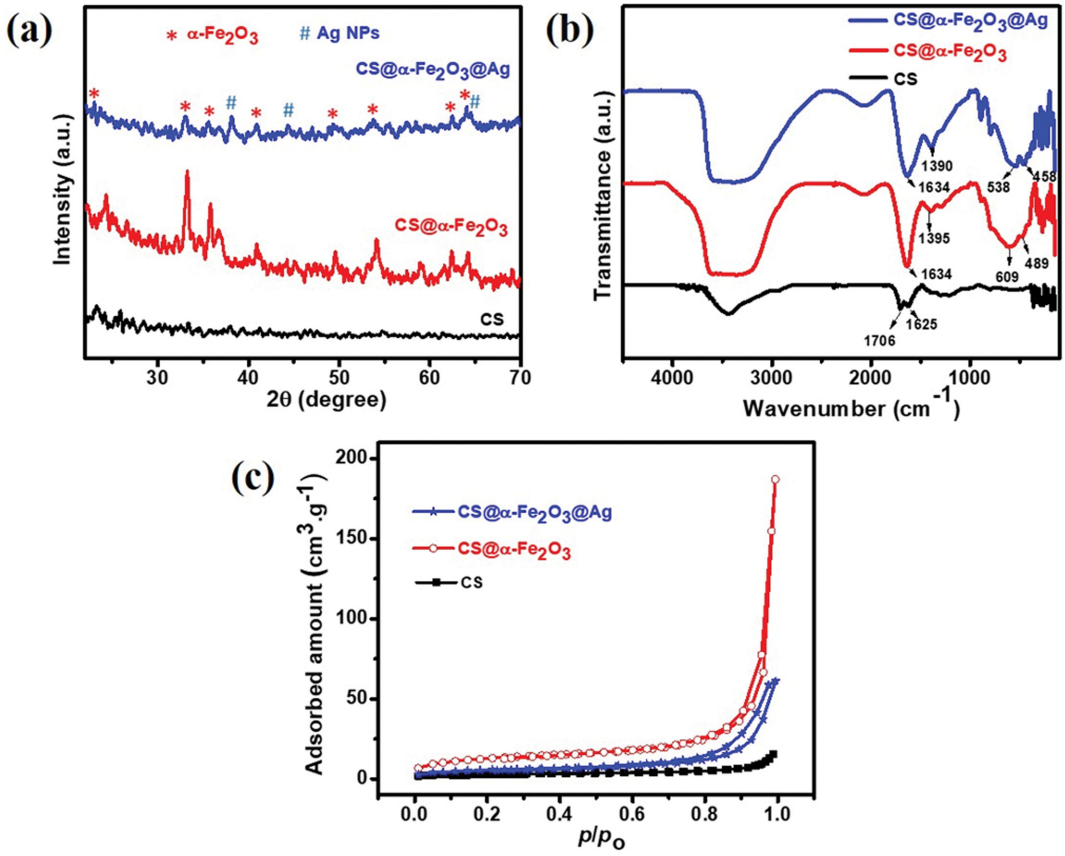

Fig. 3. (a) XRD patterns, (b) FT-IR spectra, and (c) N_2 sorption of CS, CS@α-Fe_2O_3, and CS@α-Fe_2O_3@Ag.

corresponding to (111) and (200) planes, respectively. It has been reported that incorporating Ag NPs onto the matrix of α-Fe_2O_3 shell layer can improve the prepared material's electrical conductivity and electrochemical performance process [27].

Crystallographic analyses of CS, CS@α-Fe_2O_3, and CS@α-Fe_2O_3@Ag nanocomposites are shown in Fig. 3(a). No diffraction peaks were witnessed on the XRD pattern of CS, suggesting that the prepared CS had an amorphous structure. On the other hand, the XRD pattern of CS@α-Fe_2O_3 showed high-intensity peaks at 2θ= 24.29, 33.26, 35.83, 40.91, 49.56, 54.08, 62.40, and 64.21°, assigned to the rhombohedral α-Fe_2O_3 (JCPDS card No. 33-0064). Meanwhile, the XRD pattern of the CS@α-Fe_2O_3@Ag composite exhibited new diffraction peaks of 38.13°, 44.31°, and 64.31°, attributable to Ag NPs (JCPDS card No.04-0783). Notably, the diffraction peaks of α-Fe_2O_3 on the XRD pattern of CS@α-Fe_2O_3@Ag slightly shifted left, and its intensity decreased, attributable to the incorporation of Ag NPs into the matrix of α-Fe_2O_3. The functional group analyses of CS, CS@α-Fe_2O_3, and CS@α-Fe_2O_3@Ag are shown in Fig. 3(b). The FT-IR spectrum of the CS sample exhibited peaks at ~1,706 and 1,625 cm^{-1}, attributed to the stretching vibration of COO^- and C=C groups in carbon microspheres, respectively [28]. These peaks slightly shifted toward the lower wavenumber area on the FT-IR spectra of CS@α-Fe_2O_3 and CS@α-Fe_2O_3@Ag samples. This could be because the carboxylate groups of CSs interact with Fe in α-Fe_2O_3. The spectrum of the CS@α-Fe_2O_3 sample showed vibrational modes around ~609 and 485 cm^{-1}, which were ascribed to the bending vibrations of the Fe-O bonds of α-Fe_2O_3 [29]. The peaks also shifted to 538 and 458 cm^{-1} on the spectrum of the CS@α-Fe_2O_3@Ag sample. This phenomenon could be due to the incorporation of Ag NPs into the α-Fe_2O_3 shell. Fig. 3(c) shows the nitrogen adsorption-desorption isotherms of the synthesized CS, CS@α-Fe_2O_3, and CS@α-Fe_2O_3@Ag. All samples exhibited a typical type IV with a small hysteresis loop at high relative pressure, demonstrating the presence of mesopores within their structures [30]. The calculated specific surface areas of CS, CS@α-Fe_2O_3, and CS@α-Fe_2O_3@Ag were ~12, 51, and 22 m^2 g^{-1}, respectively. The construction of the α-Fe_2O_3 layer shell on the CS increased the specific surface areas of the resultant materials.

2. Electrochemical Performance of Different Electrodes

GCEs modified with CS, CS@α-Fe_2O_3, and CS@α-Fe_2O_3@Ag were applied for simultaneous detection of UA, XN, and HP in their equimolar solution through CV experiment at a scan rate of 200 mVs^{-1}, with the potential ranging from −0.2 to 1.4 V. An equimolar mixture containing UA, XN, and HP prepared with 0.2-M BR-BS pH 7 was used. Fig. 4 compares the oxidation peak currents for UA, XN, and HP with different electrodes, revealing that the fabricated CS@α-Fe_2O_3@Ag-modified GCE exhibited the highest oxidation peak currents for all components. These findings indicate that the fabricated ternary core-shell composite CS@α-Fe_2O_3@Ag had more excellent electrochemical performance than its counterparts.

The electroactive surface area of CS@α-Fe_2O_3@Ag-modified GCE was determined using Randles-Sevcik equation as follows [31]:

$$I_p=(2.69\times10^5)\cdot n^{3/2}\cdot A\cdot C\cdot D^{1/2}\cdot v^{1/2}, \quad (3)$$

where I_p refers to the anodic or cathodic peak current (μA), D is

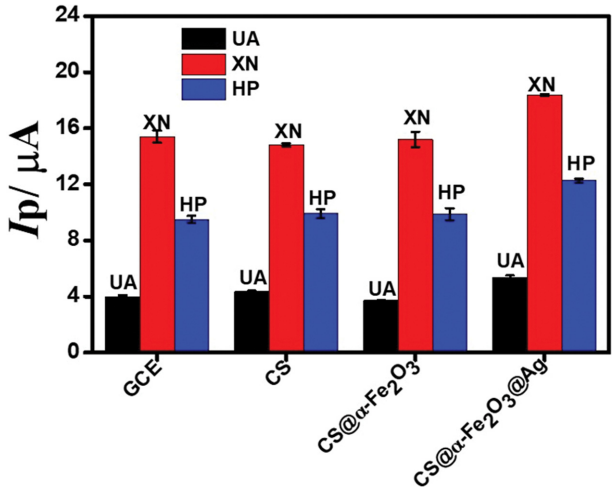

Fig. 4. The oxidation peak currents of bare GCE, and the GCEs coated with CS, CS@α-Fe_2O_3, and CS@α-Fe_2O_3@Ag in a solution containing UA, XN, and HP (10^{-4} M).

the diffusion coefficient of $K_3[Fe(CN)_6]/K_4[Fe(CN)_6]$ (1 mM) in KCl (0.1 M), C is the concentration of the $K_3[Fe(CN)_6]/K_4[Fe(CN)_6]$ (mM); A is the electroactive area (cm^2), n is the number of transferred electrons, and v is the scan rate (V s^{-1}). Fig. 5 shows the plot of I_p as a function of the scan rate V of bare GCE, CS-modified GCE, CS@α-Fe_2O_3-modified GCE, and CS@α-Fe_2O_3@Ag-modified GCE. Accordingly, their corresponding electroactive surface area values were 0.041, 0.050, 0.054, and 0.066 cm^2, respectively. The highest electroactive surface area value obtained with the CS@α-Fe_2O_3@Ag-modified GCE confirmed its excellent electrochemical performance. This is evident because the electron transfer between the electrode surface and electrolytes was accelerated when the surface of the GCE was coated by the core-shell spheres of CS@α-Fe_2O_3@Ag. Herein, the combination of α-Fe_2O_3 and Ag NPs synergistically enhanced the sensing performance activity owing to their excellent chemical compatibility and good conductivity.

Effects of pH media and scan rate on the electrochemical performance that occurred at the surface of the CS@α-Fe_2O_3@Ag-modified GC electrode were investigated. Fig. 6 shows the CV of UA, XN, and HP on the modified electrode measured at pH=3 to 5 [Fig. 6(a)] and at pH=6 to 11 [Fig. 6(b)]. As shown in Fig. 6(a), the oxidation peak of HP was unobserved when the pH ranged from 3 to 5. However, at a higher pH value (>6), the current for UA, XN, and HP increased and reached the maximum value at pH=7. In addition, their peak potential shifted toward the negative potential area, evidencing the direct involvement of protons in the oxidation process [Figs. 6(b)-(c)]. Fig. 6(d) shows the linear relationship between the anodic peak potential and pH value obtained for UA, XN, and HP, respectively; their corresponding slope values were 0.061, 0.061, and 0.059, respectively. These values were quite close to the Nernst equation, suggesting that the number of protons and electrons involved in the oxidation process on the CS@α-Fe_2O_3@Ag-modified GCE was equal.

The effects of scan rate on the electrochemical performance of the CS@α-Fe_2O_3@Ag-modified GC electrode were revealed through the relationship between scan rate and oxidation peak current. Upon

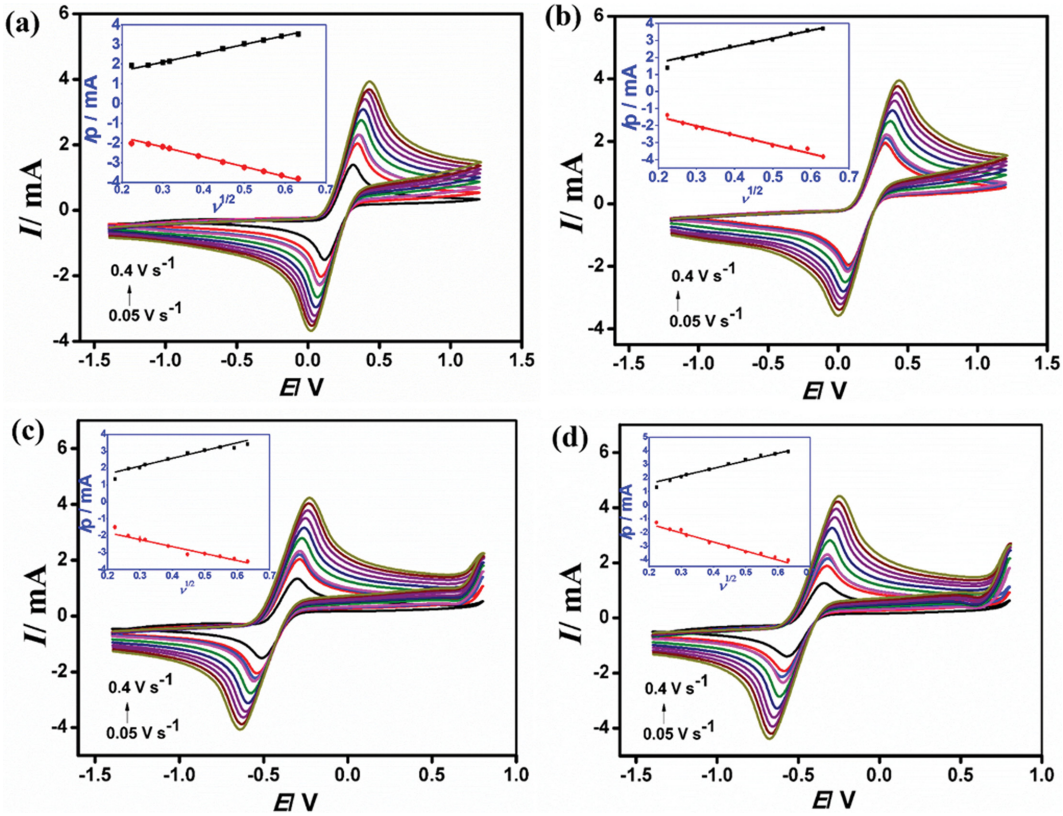

Fig. 5. Cyclic voltammogram response and the corresponding plots of peak currents *vs.* square root of scan rate (0.1-mM $K_3[Fe(CN)_6]$/ $K_4[Fe(CN)_6]$ in 0.1-M KCl) of (a) bare GCE, (b) CS-coated GCE, (c) CS@α-Fe_2O_3-coated GCE, and (d) CS@α-Fe_2O_3@Ag-coated GCE.

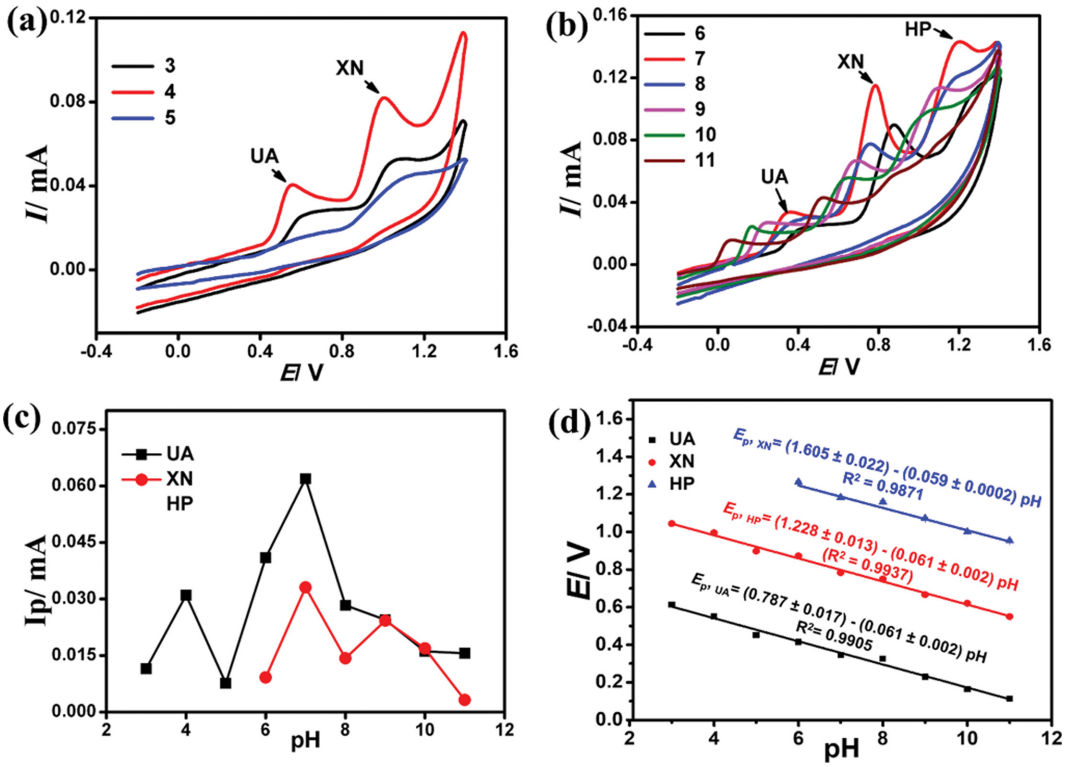

Fig. 6. Cyclic voltammogram response of CS@α-Fe_2O_3@Ag-coated GCE in an equimolar solution of UA, XN, and HP (5×10^{-4} M) at: (a) pH=3 to 5, (b) pH=6 to 11, (c) the plots of peak currents (I_p) with pH values, and (d) the linear plots of E_p *vs.* pH media.

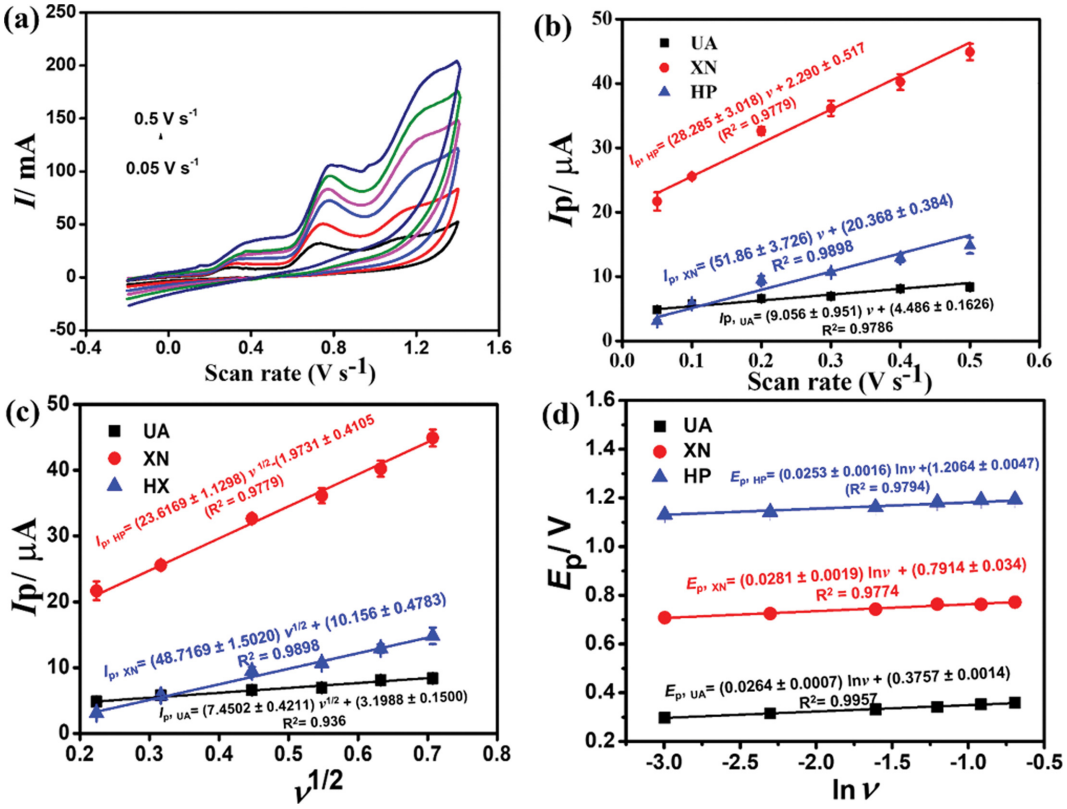

Fig. 7. (a) Cyclic voltammogram response of CS@α-Fe_2O_3@Ag-coated GCE measured in an equimolar solution of UA, XN, and HP (5×10^{-4} M) at various scan rates, (b) the plots of I_p *vs.* v, (c) plots of I_p *vs.* $v^{1/2}$, and (d) plots of E_p *vs.* lnv.

increasing the scan rate from 0.05 to 0.5 V s^{-1}, the oxidation peak potentials shifted toward the positive area, whereas the anodic peak currents for UA, XN, and HP increased linearly [Figs. 7(a)-(b)], suggesting that the oxidation of UA, XN, and HP at the CS@α-Fe_2O_3@Ag-modified electrode's surface was controlled by the adsorption process [32]. It had been reported that the electrode reaction process was considered to be a diffusion-controlled electrode process when the intercept of the plot for I_p *vs.* $v^{1/2}$ passed the origin; otherwise, it was an adsorption-controlled process [33]. The plots of I_p *vs.* $v^{1/2}$ obtained for UA, XN, and HP are shown in Fig. 7(c), confirming that the reactions of UA, XN, and HP at the surface of the electrode were driven by their adsorption process.

The number of electrons transferred can be determined by employing the Laviron equation:

$$E_p = E^0 - \frac{RT}{(1-\alpha)nF}\ln\frac{RTK_s}{(1-\alpha)nF} + \frac{RT}{(1-\alpha)nF}\ln v, \quad (4)$$

where E_0, α, and n are the formal standard potential, charge transfer coefficient, and the number of electrons transferred, respectively; F and K_s are the Faraday constant and standard heterogeneous reaction rate constant, respectively. The linear plots of E_p *vs.* lnv and the corresponding equations obtained for UA, XN, and HP are shown in Fig. 7(d). For the irreversible process (α=0.5), the numbers of electrons transferred were ~1.944, 1.826, and 2.030 for UA, XN, and HP, respectively, which suggested that two electrons were involved in the redox process [34]. Based on the obtained results, possible mechanisms for the oxidation of UA, XN, and HP at the CS@α-Fe_2O_3@Ag-coated GCE surface are described in Fig. 8.

3. Stability, Repeatability, and Detection Limit of CS@α-Fe_2O_3@Ag-coated GCE

Stability and repeatability tests using the prepared CS@α-Fe_2O_3@Ag-modified GC electrode were implemented using the DPV method with 0.2-M Britton-Robinson buffer solutions (pH 7). After each measurement, the electrode was preserved in DI water before reuse. Fig. 9(a) shows the oxidation peak currents observed for the equimolar mixture containing UA, XN, and HP (5×10^{-4} M) during 15 days, revealing a slight decrease of ~10% in peak currents. This finding suggested that the fabricated CS@Fe_2O_3@Ag-modified GCE had good stability. In addition, a series of ten consecutive DPV measurements using the CS@α-Fe_2O_3@Ag-modified GCE showed that there was only an insignificant change in their oxidation peak potentials [Fig. 9(b)]. Differential pulse voltammograms of different equimolar solutions of UA, XN, and HP were recorded to determine the limit of detection (LOD) of the CS@α-Fe_2O_3@Ag-modified GCE [Fig. 9(c)]. The corresponding linear plots of I_p *vs.* concentration of the three tested compounds are shown in Fig. 9(d). LOD is defined as the minimum detectable amount of analyte using the developed electrode, calculated using the LOD=3S/b equation [35], where S is the standard deviation of the lowest concentration of UA, XN, and HP; b is the slope of the calibration curve obtained from the DPV. Accordingly, the LOD values obtained for UA, XN, and HP at the surface of CS@Fe_2O_3@Ag-modified GCE were found to be ~0.042, 0.089, and 0.048 μmol L^{-1}, respectively, surpassing many other previously designed electrodes, such as $Ru(DMSO)_4Cl_2$-

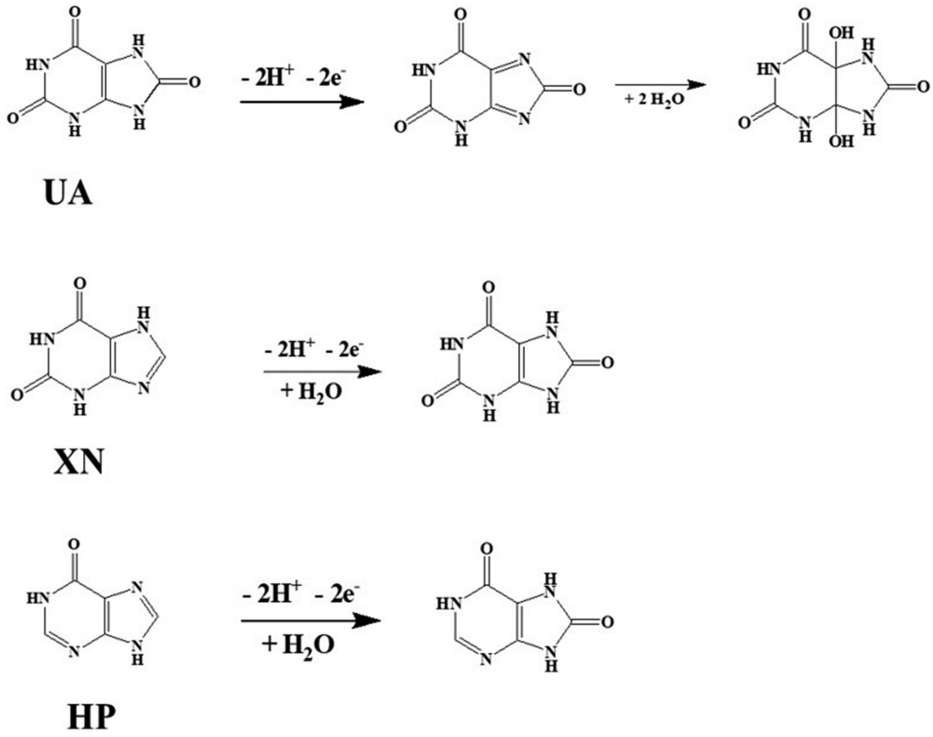

Fig. 8. The oxidation reactions of UA, XN, and HP at CS@α-Fe_2O_3@Ag-coated GCE.

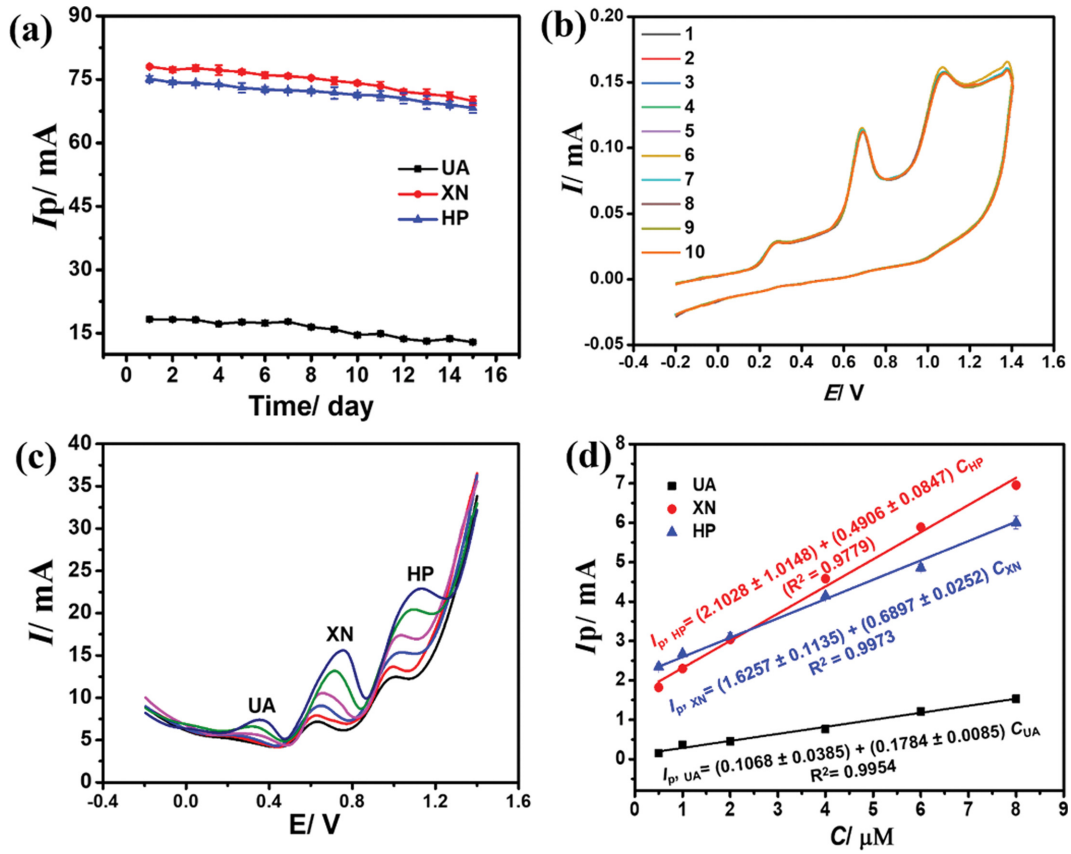

Fig. 9. Stability test and detection limit of CS@α-Fe_2O_3@Ag-coated GCE: (a) Oxidation peak currents measured for 15 days, (b) 10 consecutive DPV measurements, (c) DPV in different equimolar solutions of UA, XN, and HP with concentrations ranging from 0.5 to 8.0 μmol L^{-1}, and (d) the plots of anodic peak currents as a function of analyte concentration.

Table 1. Comparison between the CS@α-Fe_2O_3@Ag-coated GCE and other modified GCEs in the simultaneous determination of UA, XN, and HP

Electrode modifier	Analytes	Linear range (μM)	LOD (μM)	References
Ru $(DMSO)_4Cl_2$ nanoaggregated Nafion	UA	100-700	0.372	[36]
	XN	50-500	2.35	
	HP	50-300	2.37	
Preanodized nontronite	UA	2.0-40	0.42	[37]
	XN	2.0-40	0.07	
	HP	4.0-30	0.34	
Poly (bromocresol purple)	UA	0.5-120	0.20	[38]
	XN	0.1-100	0.06	
	HP	20-80	0.12	
Poly(pyrocatechol violet)/ functionalized multi-walled carbon nanotubes composite	UA	0.3-80	0.16	[12]
	XN	0.1-100	0.05	
	HP	0.5-90	0.20	
Graphitized mesoporous carbon	UA	20-40	0.11	[9]
	XN	20-320	0.39	
	HP	20-240	0.35	
CS@*a*-Fe_2O_3@Ag	UA	0.5-8	0.042	This work
	XN	0.5-8	0.089	This work
	HP	0.5-8	0.048	This work

grafted Nafion, poly(bromocresol purple), or pyrolytic graphite (Table 1). The obtained results suggest that the fabricated CS@α-Fe_2O_3@Ag-modified GCE could be a promising electrode for detecting UA, XN, and HP.

CONCLUSIONS

CS@α-Fe_2O_3@Ag composites were successfully fabricated via multistep hydrothermal synthesis. The prepared CS@α-Fe_2O_3@Ag composites exhibited a heterojunction hierarchical core-shell structure and improved porosity. In addition, the GCE surface coated with CS@ α-Fe_2O_3@Ag composites showed more excellent electrochemical properties than the bare GCE. The simultaneous voltammetric detection of UA, XN, and HP using the CS@α-Fe_2O_3@Ag-coated GCE revealed that their linear concentration ranged from 0.5 to 8.0 μmol L^{-1}, with LOD of 0.042, 0.089, and 0.048 μmol L^{-1}, respectively. Moreover, the CS@α-Fe_2O_3@Ag-coated GCE also had good stability and repeatability. Thus, it is a promising electrode for the simultaneous analysis of UA, XN, and HP.

ACKNOWLEDGEMENTS

This work was supported by the Basic Science Research Program (NRF-2019R1A2C1090693) and the Engineering Research Center of Excellence Program (NRF-2021R1A5A6002853) through the National Research Foundation (NRF) funded by the Ministry of Science and ICT, Republic of Korea, and the Industrial University of Ho Chi Minh City, Vietnam [21.2CNHSV01].

The first author was funded by Vingroup JSC and supported by the Master, PhD Scholarship Programme of Vingroup Innovation Foundation (VINIF), Institute of Big Data [VINIF.2021.TS.080].

REFERENCES

1. M. Labib, E. H. Sargent and S. O. Kelley, *Chem. Rev.*, **116**, 9001 (2016).
2. M. Alderman and K. J. V. Aiyer, *Curr. Med. Res. Opin.*, **20**, 369 (2004).
3. Z. Yan, Q. Niu, M. Mou, Y. Wu, X. Liu and S. Liao, *J. Nanoparticle Res.*, **19**, 1 (2017).
4. N. Nuchtavorn, W. Suntornsuk, S. M. Lunte and L. Suntornsuk, *J. Pharm. Biomed. Anal.*, **113**, 72 (2015).
5. R. Sakthivel, B. Mutharani, S. Chen, S. Kubendhiran, T. Chen, F. M. A. Al-Hemaid, M. A. Ali and M. S. Elshikh, *J. Electrochem. Soc.*, **165**, B422 (2018).
6. J. V. Kumar, R. Karthik, S. M. Chen, S. Marikkani, A. Elangovan and V. Muthuraj, *J. Colloid Interface Sci.*, **496**, 78 (2017).
7. M. Keyvanfard, R. Shakeri, H. Karimi-Maleh and K. Alizad, *Mater. Sci. Eng. C*, **33**, 811 (2013).
8. M. Blanco and M. Alcalá, *Eur. J. Pharm. Sci.*, **27**, 280 (2006).
9. R. Thangaraj and A. S. Kumar, *Anal. Methods*, **4**, 2162 (2012).
10. A. Luo, Q. Lian, Z. An, Z. Li, Y. Guo, D. Zhang, Z. Xue, X. Zhou and X. Lu, *J. Electroanal. Chem.*, **756**, 22 (2015).
11. N. Lavanya, C. Sekar, R. Murugan and G. Ravi, *Mater. Sci. Eng. C*, **65**, 278 (2016).
12. Y. Wang, *Colloids Surf. B Biointerfaces*, **88**, 614 (2011).
13. Y. Jiao, Y. Liu, B. Yin, S. Zhang, F. Qu and X. Wu, *Nano Energy*, **10**, 90 (2014).
14. Z. Yan, Y. Kang, D. Li and Y. C. Liu, *Korean J. Chem. Eng.*, **37**, 623 (2020).
15. C. H. Tang, X. Yin and H. Gong, *ACS Appl. Mater. Interfaces*, **5**, 10574 (2013).
16. X. Sun, T. Xu, J. Bai and C. Li, *ACS Appl. Energy Mater.*, **2**, 8675 (2019).

17. X. Huang, M. Kim, H. Suh and I. Kim, *Korean J. Chem. Eng.*, **33**, 2228 (2016).
18. L. Bao, J. Zang and X. Li, *Nano Lett.*, **11**, 1215 (2011).
19. L. Zhang, H. Bin Wu, S. Madhavi, H. H. Hng and X. W. Lou, *J. Am. Chem. Soc.*, **134**, 17388 (2012).
20. B. Wang, J. S. Chen, H. Bin Wu, Z. Wang and X. W. Lou, *J. Am. Chem. Soc.*, **133**, 17146 (2011).
21. K. K. Lee, S. Deng, H. M. Fan, S. Mhaisalkar, H. R. Tan, E. S. Tok, K. P. Loh, W. S. Chin and C. H. Sow, *Nanoscale*, **4**, 2958 (2012).
22. J. Hu, M. Noked, E. Gillette, F. Han, Z. Gui, C. Wang and S. B. Lee, *J. Mater. Chem. A*, **3**, 21501 (2015).
23. S. S. Raut and B. R. Sankapal, *New J. Chem.*, **40**, 2619 (2016).
24. D. R. Kauffman, X. Deng, D. C. Sorescu, T. D. N. Phan, C. Wang, C. M. Marin, E. Stavitski, I. Waluyo and A. Hunt, *ACS Catal.*, **111**, 5375 (2019).
25. X. Lin, J. Zhang, X. Tong, H. Li, X. Pan, P. Ning and Q. Li, *Sci. Rep.*, **7**, 1 (2017).
26. S. M. Hwang, Y. Limb, J. Kim, Y. Heoc, J. H. Limd, Y. Yamauchie, M. S. Park, Y. Kim, S. X. Doua and J. H. Kim, *Nano Energy*, **10**, 53 (2014).
27. A. Saranya, T. Alomayri, K. Ramar, A. Priyadharsan, V. Raj, K. Murugan, M. Alsawalha and P. Maheshwaran, *J. Photochem. Photobiol. B Biol.*, **207**, 111885 (2020).
28. H. I. Adegoke, F. AmooAdekola, O. S. Fatoki and B. J. Ximba, *Korean J. Chem. Eng.*, **31**, 142 (2014).
29. J. Y. Park, S. G. Oh and B. H. Ha, *Korean J. Chem. Eng.*, **18**, 215 (2001).
30. F. J. Sotomayor, K. A. Cychosz and M. Thommes, *Acc. Mater. Surf. Res.*, **3**, 34 (2018).
31. A. M. Bagoji and S. T. Nandibewoor, *New J. Chem.*, **40**, 3763 (2016).
32. E. Laviron, *J. Electroanal. Chem.*, **101**, 19 (1979).
33. S. Yang, L. Qu, R. Yang, J. Li and L. Yu, *J. Appl. Electrochem.*, **40**, 1371 (2010).
34. J. Soleymani, M. Hasanzadeh, N. Shadjou, M. K. Jafari, J. V. Gharamaleki, M. Yadollahi and A. Jouyban, *Mater. Sci. Eng. C*, **61**, 638 (2016).
35. S. K. Ponnaiah, P. Periakaruppan and B. Vellaichamy, *J. Phys. Chem. B*, **122**, 3037 (2018).
36. A. S. Kumar and P. Swetha, *J. Electroanal. Chem.*, **642**, 135 (2010).
37. J. M. Zen, Y. Y. Lai, H. H. Yang and A. Senthil Kumar, *Sensors Actuators, B Chem.*, **84**, 237 (2002).
38. Y. Wang and L. L. Tong, *Sensors Actuators, B Chem.*, **150**, 43 (2010).